Physics-based Control-oriented Modeling of the Current Profile Evolution in NSTX-Upgrade

Zeki Ilhan[1], Justin Barton[1], Wenyu Shi[1], Eugenio Schuster[1],
David Gates[2], Stefan Gerhardt[2], Egemen Kolemen[2], Jonathan Menard[2]

[1]Department of Mechanical Engineering & Mechanics
Lehigh University

[2]Princeton Plasma Physics Laboratory

zoi210@lehigh.edu

55th Annual Meeting of the APS Division of Plasma Physics

November 13, 2013

Motivation for Current Profile Control in NSTX-U

- Some of the next-step operational goals for NSTX-Upgrade include [1]:
  - Non-inductive sustainment of the high-β spherical torus.
  - High performance equilibrium scenarios with neutral beam heating.
  - Longer pulse durations.

- **Active, model-based, feedback control** of the **current profile** evolution can be useful to achieve those stability and performance criteria.

- The **q-profile**, which is related to the **toroidal current density** in the machine, plays an important role in the stability and performance of a given magnetic configuration.

- Availability of the additional neutral beam current sources ***enables feedback control of the current profile*** in NSTX-U.

[1] GERHARDT, S. P. et al., Nuclear Fusion (2012).

Model-based Feedback Control Scheme

- The purpose of this work is to convert accepted physics-based models to a form suitable for control design.

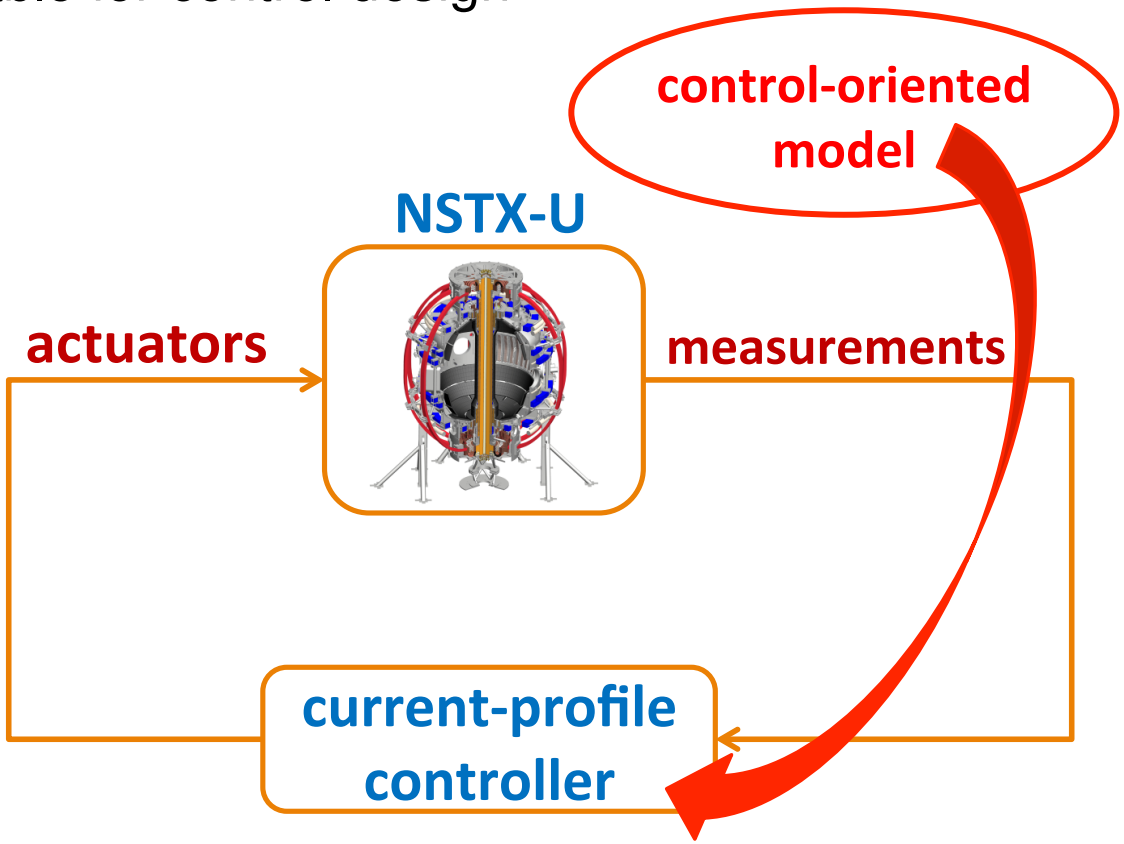

- ***Modeling for control design and not for physical understanding!***
- **The control-oriented model** only needs to **capture the dominant effects** of the actuators on the current profile evolution.
- Control-oriented model will be **embedded in current-profile controller**.

First-Principles-Driven (FPD) Current Profile Modeling

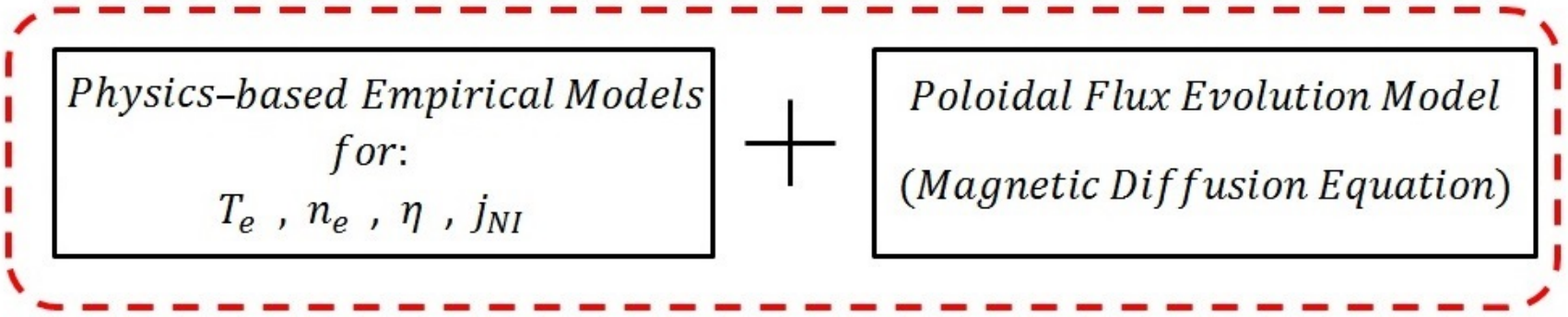

First – Principles – Driven (FPD) Current Profile Evolution Model

- **Empirical models** take a **"separation of variables"** form, i.e., the spatial-temporal dependence of plasma parameters is separated.
- Modeling of electron temperature admits different levels of approximation. Ad-hoc transport models can be parameterized and tuned to data from experiment or predictive simulations by higher-accuracy transport codes.
- Fixed 2D MHD equilibrium $\Rightarrow$ Extension to variable equilibrium possible
- Model includes **nonlinear coupling between different plasma profiles.** FPD modeling allows for **further integration** (e.g., rotation profile).
- FPD modeling approach arbitrarily handles trade-off between simplicity of model and both its physics accuracy and range of validity.

Magnetic Diffusion Equation

- Using $\Phi = \pi B_{\phi,0}\rho^2$ and $\hat{\rho} = \rho/\rho_b$, the safety factor (q-profile) is expressed as:

$$q(\hat{\rho},t) = \frac{1}{\bar{\iota}} = -\frac{d\Phi}{d\Psi} = -\frac{d\Phi}{2\pi d\psi} = -\frac{\frac{\partial\Phi}{\partial\rho}\frac{\partial\rho}{\partial\hat{\rho}}}{2\pi\frac{\partial\psi}{\partial\hat{\rho}}} = -\frac{B_{\phi,0}\rho_b^2\hat{\rho}}{\partial\psi/\partial\hat{\rho}} \tag{1}$$

- The evolution of the poloidal magnetic flux is given by [2]:

$$\frac{\partial\psi}{\partial t} = \frac{\eta(T_e)}{\mu_0\rho_b^2\hat{F}^2}\frac{1}{\hat{\rho}}\frac{\partial}{\partial\hat{\rho}}\left(\hat{\rho}\hat{F}\hat{G}\hat{H}\frac{\partial\psi}{\partial\hat{\rho}}\right) + R_0\hat{H}\eta(T_e)\frac{<\bar{j}_{NI}\cdot\bar{B}>}{B_{\phi,0}}, \tag{2}$$

  where the parameters $\hat{F}$, $\hat{G}$ and $\hat{H}$ are geometric factors pertaining to the magnetic configuration of a particular plasma equilibrium given by:

$$\hat{F} = \frac{R_0 B_{\phi,0}}{RB_\phi(R,Z)} \qquad \hat{G} = \left\langle\frac{R_0^2}{R^2}|\nabla\rho|^2\right\rangle \qquad \hat{H} = \frac{\hat{F}}{\left\langle R_0^2/R^2\right\rangle}, \tag{3}$$

- The boundary conditions are given by:

$$\left.\frac{\partial\psi}{\partial\hat{\rho}}\right|_{\hat{\rho}=0} = 0 \qquad \left.\frac{\partial\psi}{\partial\hat{\rho}}\right|_{\hat{\rho}=1} = -\frac{\mu_0}{2\pi}\frac{R_0}{\hat{G}\Big|_{\hat{\rho}=1}\hat{H}\Big|_{\hat{\rho}=1}}I(t), \tag{4}$$

[2] OU, Y., et al., Fusion Engineering and Design (2007).

Electron Density Model

- Assume tight coupling between electron and ion species in plasma, i.e., $T_e(\hat{\rho},t) \approx T_i(\hat{\rho},t)$ and $n_e(\hat{\rho},t) \approx n_i(\hat{\rho},t)$.
- Assume control action employed to regulate electron density weakly affects radial distribution of the electrons.
- Electron density $n_e(\hat{\rho},t)$ is then modeled as:

$$n_e(\hat{\rho},t) = n_e^{prof}(\hat{\rho})u_n(t) \tag{5}$$

  - $n_e^{prof}(\hat{\rho})$ is a reference electron density profile, which is the actual electron density profile taken at a reference time t_r, selected by the designer, i.e.,

$$n_e^{prof}(\hat{\rho}) = n_e(\hat{\rho},t_r) \tag{6}$$

  - $u_n(t)$ regulates time evolution of electron density.

- In this work, electron density is considered as an uncontrolled but measurable input. This decision is motivated by the fact that tight control of $n_e(\hat{\rho},t)$ in experiments is in general very challenging.

Electron Temperature Model

- Slowly evolving electron temperature profile evolution modeled as:

$$T_e(\hat{\rho},t) = \begin{cases} k_{T_e}(\hat{\rho},t_r)\left[T_e^{prof}(\hat{\rho},t_r) - T_e^{prof}(\hat{\rho}_{tb},t_r)\right] \\ \times I(t)^{\alpha} P_{tot}(t)^{\gamma} n_e(\hat{\rho},t)^{\lambda} + T_e^{prof}(\hat{\rho}_{tb},t_r), & 0 \le \hat{\rho} \le \hat{\rho}_{tb} \\ T_e^{prof}(\hat{\rho},t_r), & \hat{\rho}_{tb} < \hat{\rho} \le 1 \end{cases} \quad (7)$$

  - $T_e^{prof}(\hat{\rho},t_r)$ is the electron temperature profile taken at the reference time, t_r, $\hat{\rho}_{tb}$ is the spatial location of the transport barrier in the plasma, $I(t)$ is the plasma current, $P_{tot}(t)$ is the total power and α, γ and λ are constants.
  - The temperature profile model constant k_{T_e} in (7) is defined as

$$k_{T_e}(\hat{\rho},t_r) = \frac{n_e(\hat{\rho},t_r)}{I(t_r)\sqrt{P_{tot}(t_r)}} \quad (8)$$

- In this work, $\hat{\rho}_{tb} = 1$. Based on the T_e profile evolution, the model constants in (7) are chosen as $\alpha = 1$, $\gamma = 0.5$ and $\lambda = -1$. Therefore the T_e model (7) takes the final form

$$T_e(\hat{\rho},t) = k_{T_e}(\hat{\rho},t_r)\frac{T_e^{prof}(\hat{\rho},t_r)}{n_e(\hat{\rho},t)} I(t)\sqrt{P_{tot}(t)}, \quad (0 \le \hat{\rho} \le 1) \quad (9)$$

Total Injected Power Model

- **Total power** $P_{tot}(t)$ expressed as:

$$P_{tot}(t) = P_{ohm}(t) + P_{aux}(t) - P_{rad}(t) \tag{10}$$

- **Ohmic power** expressed as:

$$P_{ohm}(t) = \int_0^1 j_{tor}^2(\hat{\rho}, t)\eta(\hat{\rho}, t)\frac{dV}{d\hat{\rho}}d\hat{\rho} \approx \mathcal{R}(t)I_p(t)^2, \tag{11}$$

  - $j_{tor}(\hat{\rho}, t)$ is the total toroidal current density,
  - $\mathcal{R}$ is global plasma resistance, which is expressed as:

$$\mathcal{R}(t) \approx 2\pi R_0 \Big/ \int_{\hat{\rho}} \left[\frac{1}{\eta(\hat{\rho}, t)}\frac{dS}{d\hat{\rho}}d\hat{\rho}\right],$$

    where S denotes a magnetic surface within the plasma.

Auxiliary, Radiative Power and Plasma Resistivity

- **Auxiliary power** expressed as:

$$P_{aux}(t) = P_{nbitot}(k) = \sum_{k=1}^{6} P_{nbik}(t) \tag{12}$$

- **Radiative power** modeled as:

$$P_{rad}(t) = \int_0^1 Q_{rad}(\hat{\rho}, t) \frac{dV}{d\hat{\rho}} d\hat{\rho}, \tag{13}$$

where the radiative power density Q_{rad} is modeled as

$$Q_{rad}(\hat{\rho}, t) = k_{brem} Z_{eff} n_e(\hat{\rho}, t)^2 \sqrt{T_e(\hat{\rho}, t)}, \tag{14}$$

with Z_{eff} being the effective average charge of the ions in the plasma.

- **Plasma resistivity** $\eta(T_e)$ scales with electron temperature as:

$$\eta(\hat{\rho}, t) = \frac{k_{sp}(\hat{\rho}, t_r) Z_{eff}}{T_e(\hat{\rho}, t)^{3/2}}, \tag{15}$$

where k_{sp} is a constant.

Accurate Models Used for Noninductive Current Drive

- **Total noninductive current drive** in NSTX-U is produced by **neutral beam injection** via the individual beamlines and **bootstrap current:**

$$\frac{\langle \bar{j}_{ni} \cdot \bar{B} \rangle}{B_{\phi,0}} = \sum_{i=1}^{6} \frac{\langle \bar{j}_{nbi_i} \cdot \bar{B} \rangle}{B_{\phi,0}} + \frac{\langle \bar{j}_{bs} \cdot \bar{B} \rangle}{B_{\phi,0}}, \tag{16}$$

- The noninductive toroidal current density provided by each individual neutral beam injector is modeled as

$$\frac{\langle \bar{j}_i \cdot \bar{B} \rangle}{B_{\phi,0}}(\hat{\rho},t) = k_i^{prof}(\hat{\rho}) j_i^{dep}(\hat{\rho}) \frac{\sqrt{T_e(\hat{\rho},t)}}{n_e(\hat{\rho},t)} P_i(t), \quad (i = 1,2,...6) \tag{17}$$

  - k_i^{prof} are constants and $j_i^{dep}(\hat{\rho})$ are reference deposition profiles evaluated at the reference time, t_r.

- Bootstrap current drive expressed as [3], [4]:

$$\frac{\langle \bar{j}_{bs} \cdot \bar{B} \rangle}{B_{\phi,0}}(\hat{\rho},t) = \frac{k_{JeV} R_0}{\hat{F}(\hat{\rho})} \left(\frac{\partial \psi}{\partial \hat{\rho}} \right)^{-1} \left[2\mathcal{L}_{31} T_e \frac{\partial n_e}{\partial \hat{\rho}} + \{2\mathcal{L}_{31} + \mathcal{L}_{32} + \alpha \mathcal{L}_{34}\} n_e \frac{\partial T_e}{\partial \hat{\rho}} \right] \tag{18}$$

  - $\mathcal{L}_{31}(\hat{\rho})$, $\mathcal{L}_{32}(\hat{\rho})$, $\mathcal{L}_{34}(\hat{\rho})$, $\alpha(\hat{\rho})$ are function of trapped fraction and collisionality.

[3] SAUTER, O. et al., Physics of Plasmas (1999).
[4] SAUTER, O. et al., Physics of Plasmas (2002).

CASE 1: Model Tailored for NSTX-U Run 142301M21

- **NOTE: NSTX-U run 142301M21 is a TRANSP run with the NSTX-U shape and actuators, using the scaled profiles from NSTX.**

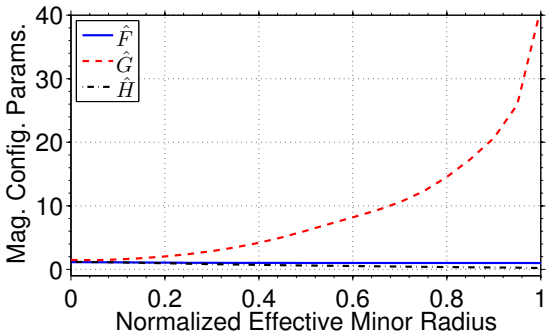

(a) $\hat{F}(\hat{\rho})$, $\hat{G}(\hat{\rho})$, $\hat{H}(\hat{\rho})$

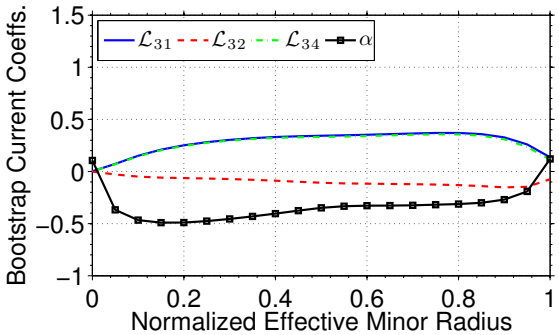

(b) $\mathcal{L}_{31}(\hat{\rho})$, $\mathcal{L}_{32}(\hat{\rho})$, $\mathcal{L}_{34}(\hat{\rho})$, $\alpha(\hat{\rho})$

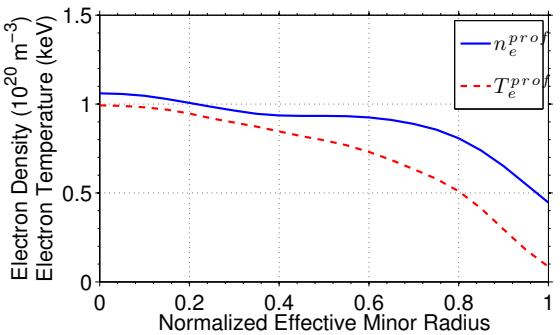

(c) $n_e^{prof}(\hat{\rho})$, $T_e^{prof}(\hat{\rho})$

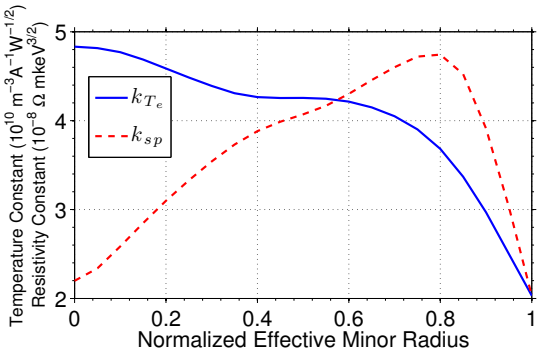

(d) $k_{T_e}(\hat{\rho})$, $k_{sp}(\hat{\rho})$

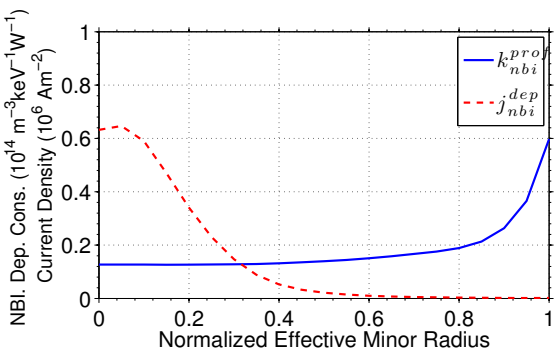

(e) $k_{nbi}^{prof}(\hat{\rho})$, $j_{nbi}^{dep}(\hat{\rho})$

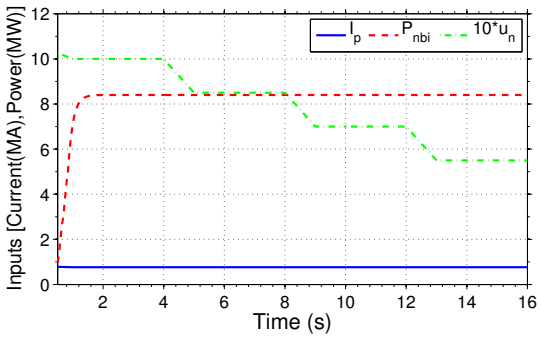

(f) Control Inputs

Fig. 1: Reference (a) magnetic configuration parameters, (b) bootstrap current coefficients, (c) electron density and temperature profiles, (d) electron temperature and plasma resistivity constants, (e) total NB deposition profile and NB model constant and (f) control inputs

Qualitative Agreement of Various Plasma Profiles in between the FPD Model and TRANSP Output

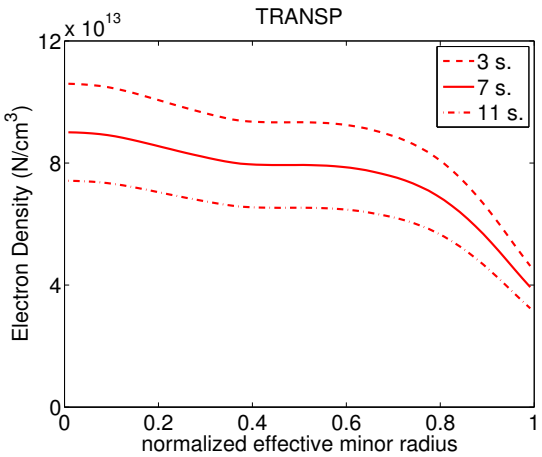

(a) $n_e(\hat{\rho})$

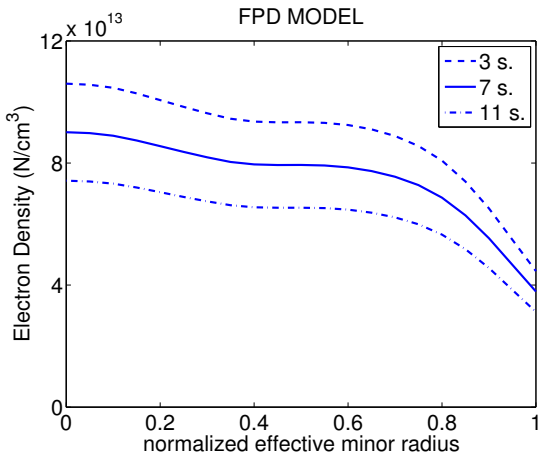

(b) $n_e(\hat{\rho})$

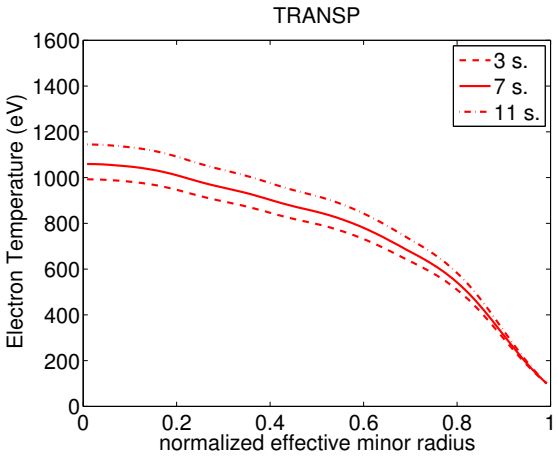

(c) $T_e(\hat{\rho})$

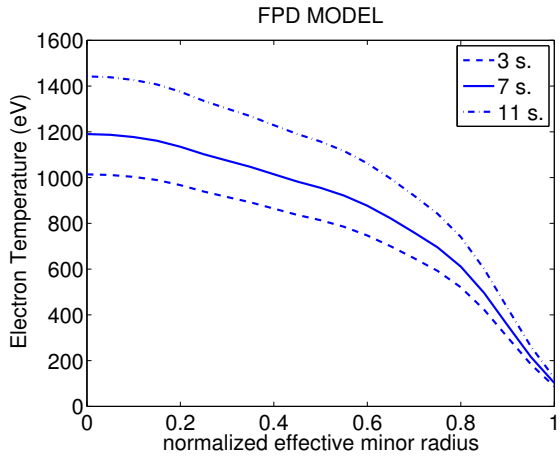

(d) $T_e(\hat{\rho})$

Fig. 2: Comparison of the T_e and n_e profiles: TRANSP [(a),(c)], FPD model [(b),(d)].

Noninductive Current Density Profile Comparison

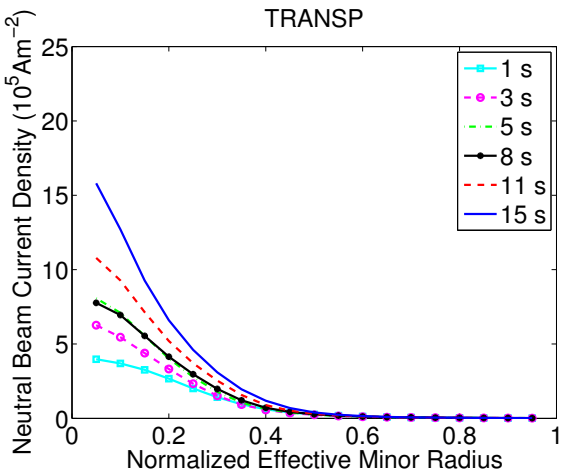

(a) Total Neutral Beam

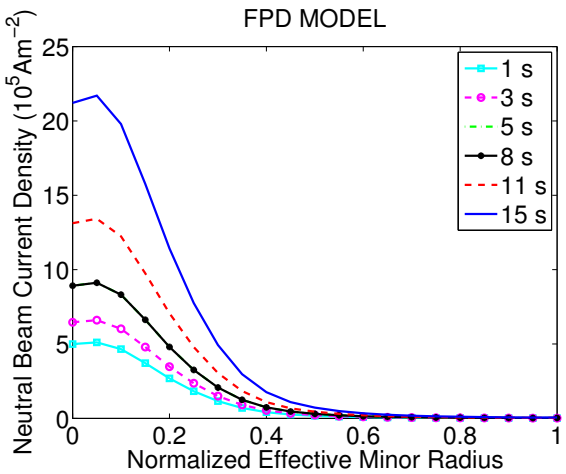

(b) Total Neutral Beam

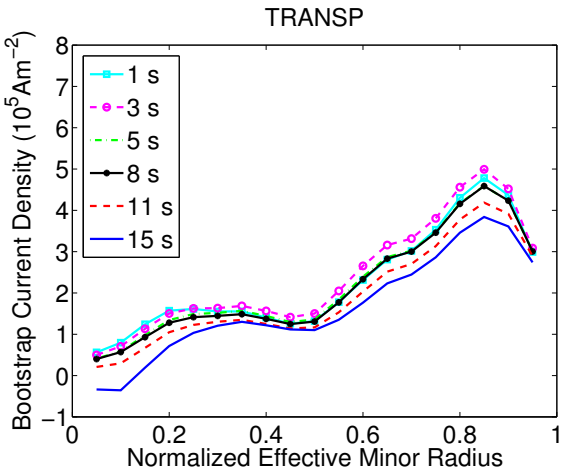

(c) Bootstrap

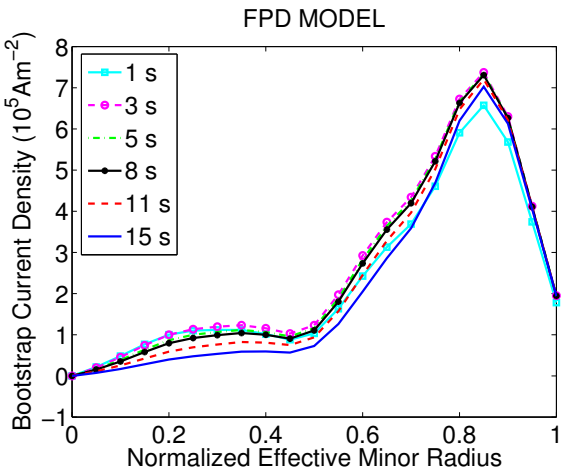

(d) Bootstrap

Fig. 3: Noninductive current deposition profile evolution comparison: TRANSP [(a),(k)], control-oriented model [(b),(l)].

Poloidal Flux Profile Comparison - $\psi(\hat{\rho})$, at fixed time

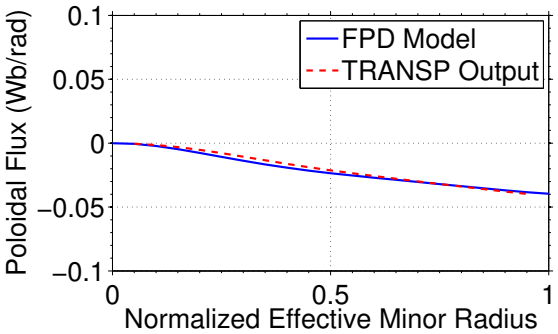

(a) $t = 1$ sec.

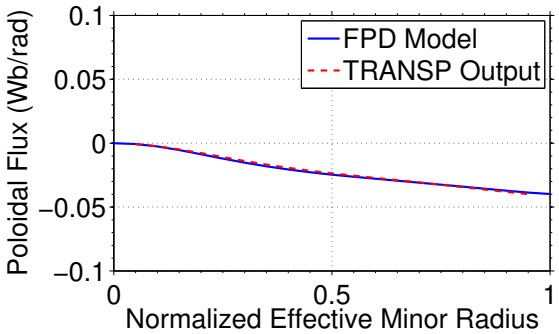

(b) $t = 3$ sec.

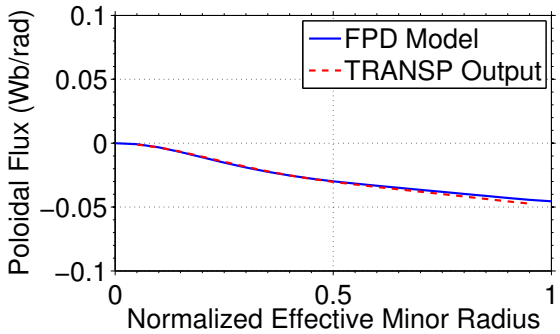

(c) $t = 6$ sec.

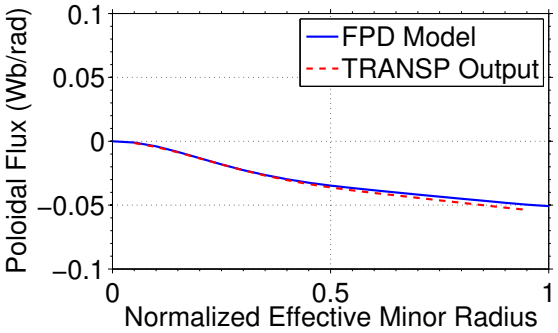

(d) $t = 9$ sec.

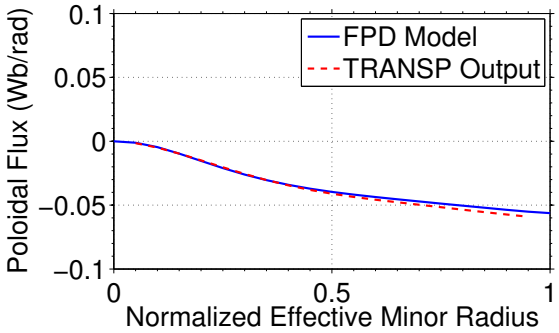

(e) $t = 12$ sec.

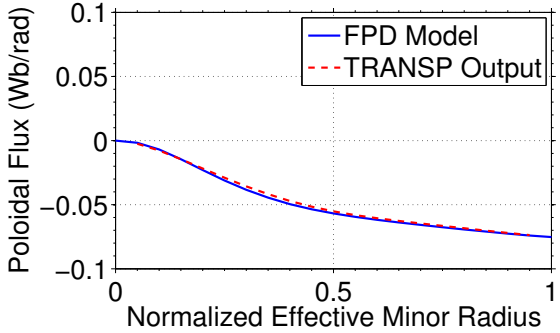

(f) $t = 15$ sec.

Fig. 4: Poloidal magnetic flux profile evolution comparison.

Poloidal Flux Comparison - $\psi(t)$, at fixed radius

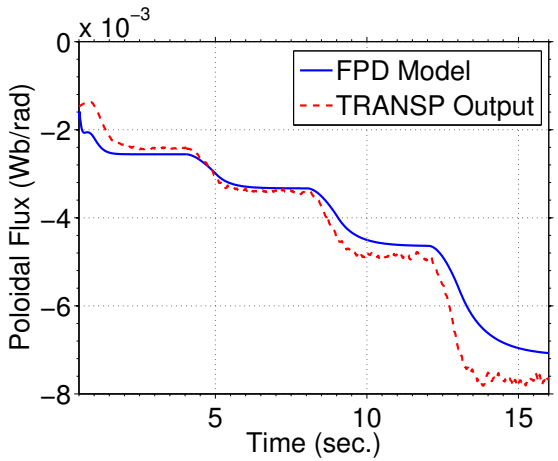

(a) $\hat{\rho} = 0.1$

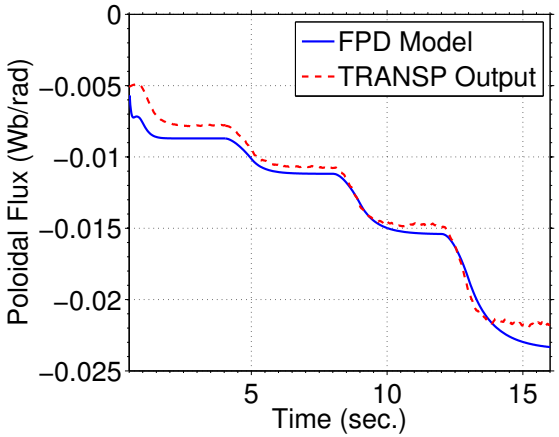

(b) $\hat{\rho} = 0.2$

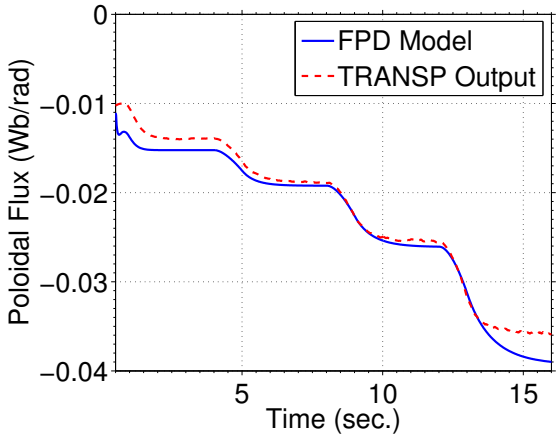

(c) $\hat{\rho} = 0.3$

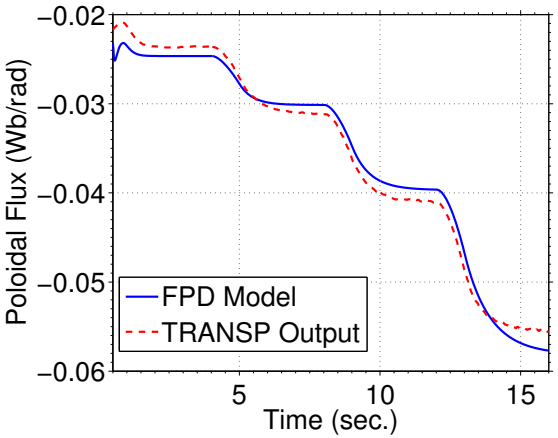

(d) $\hat{\rho} = 0.5$

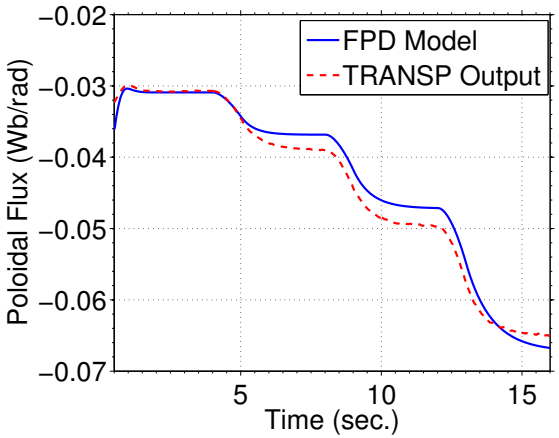

(e) $\hat{\rho} = 0.7$

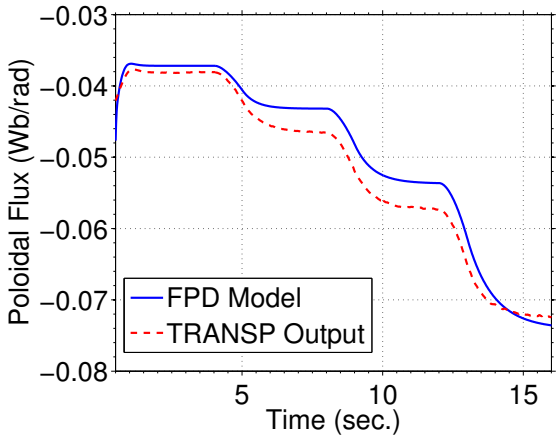

(f) $\hat{\rho} = 0.9$

Fig. 5: Poloidal magnetic flux evolution comparison.

Safety Factor Profile Comparison - $q(\hat{\rho})$, at fixed time

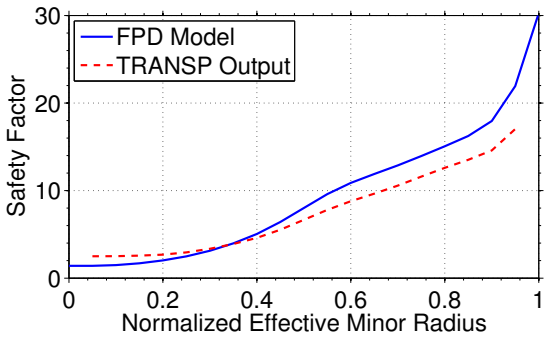

(a) $t = 1$ sec.

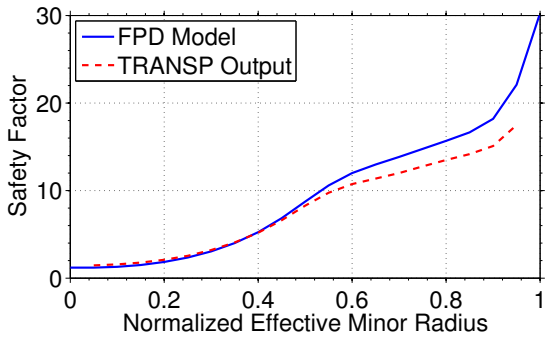

(b) $t = 3$ sec.

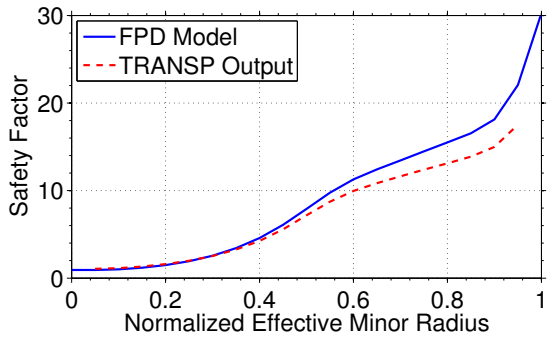

(c) $t = 6$ sec.

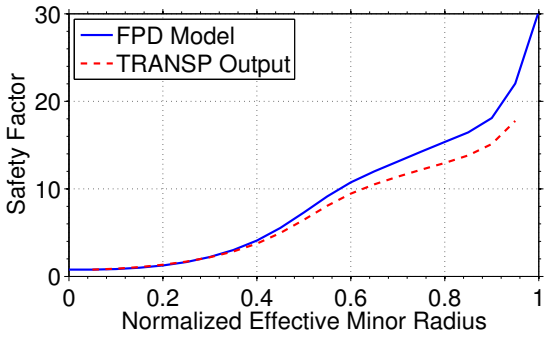

(d) $t = 9$ sec.

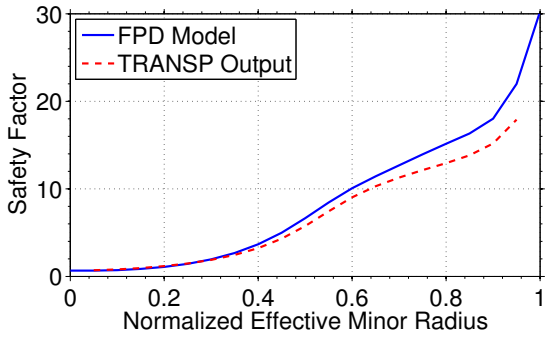

(e) $t = 12$ sec.

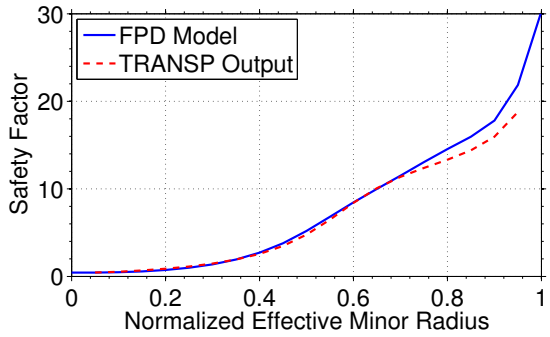

(f) $t = 15$ sec.

Fig. 6: Safety factor profile evolution comparison.

Safety Factor Comparison - $q(t)$ at fixed radius

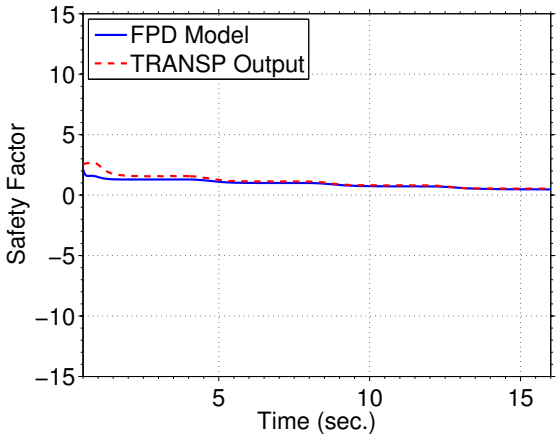

(a) $\hat{\rho} = 0.1$

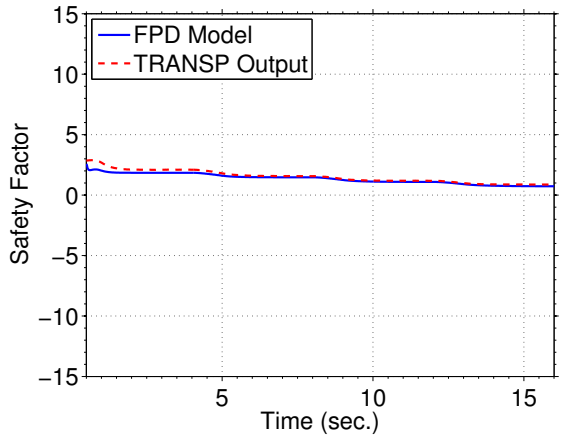

(b) $\hat{\rho} = 0.2$

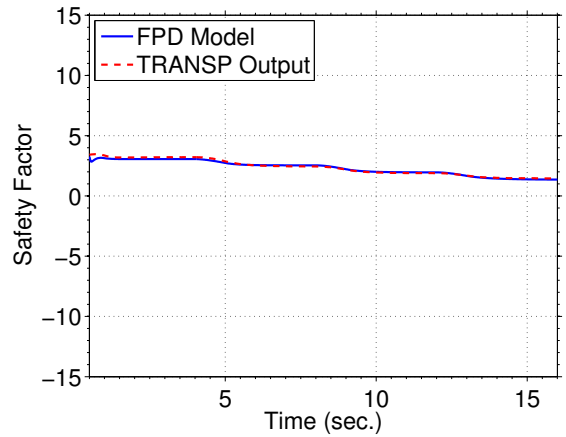

(c) $\hat{\rho} = 0.3$

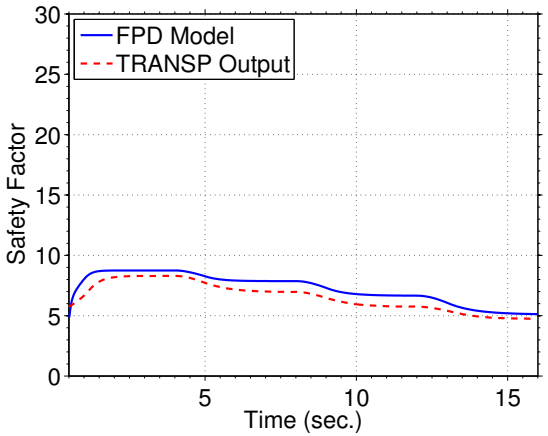

(d) $\hat{\rho} = 0.5$

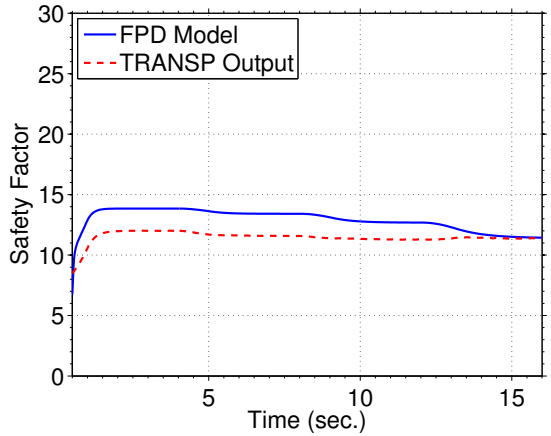

(e) $\hat{\rho} = 0.7$

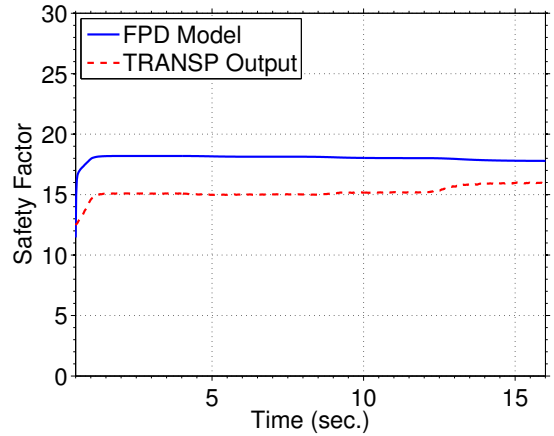

(f) $\hat{\rho} = 0.9$

Fig. 7: Safety factor evolution comparison.

CASE 2: Model Tailored for NSTX Run 133964D02

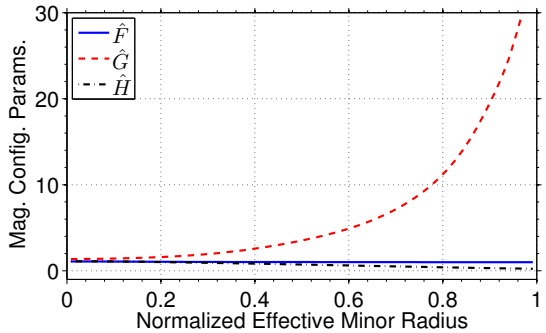

(a) $\hat{F}(\hat{\rho})$, $\hat{G}(\hat{\rho})$, $\hat{H}(\hat{\rho})$

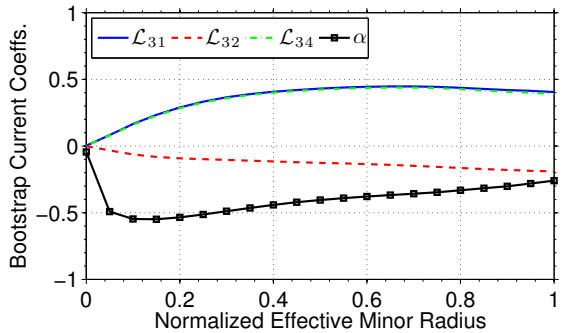

(b) $\mathcal{L}_{31}(\hat{\rho})$, $\mathcal{L}_{32}(\hat{\rho})$, $\mathcal{L}_{34}(\hat{\rho})$, $\alpha(\hat{\rho})$

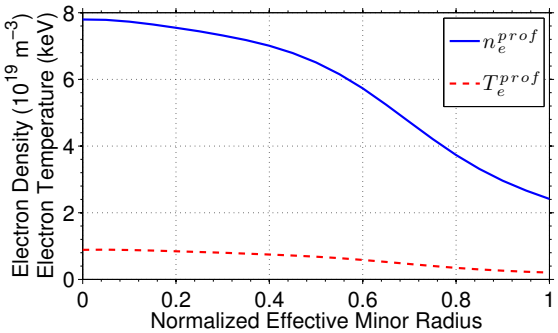

(c) $n_e^{prof}(\hat{\rho})$, $T_e^{prof}(\hat{\rho})$

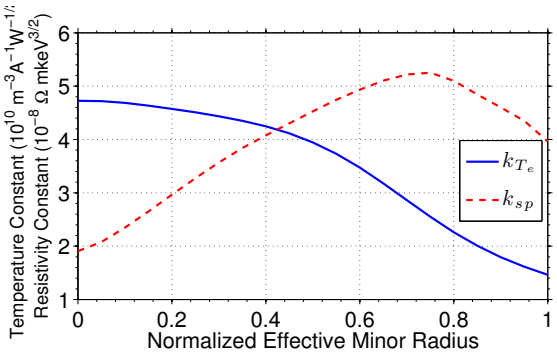

(d) $k_{T_e}(\hat{\rho})$, $k_{sp}(\hat{\rho})$

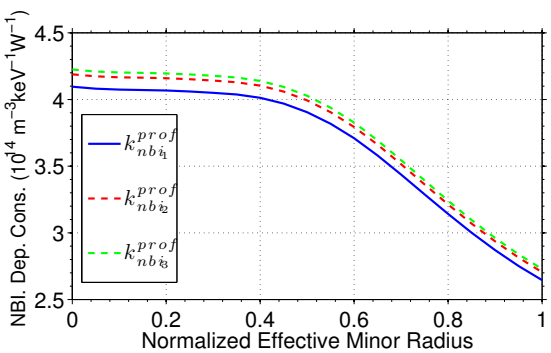

(e) $k_{nbi}^{prof}(\hat{\rho})$

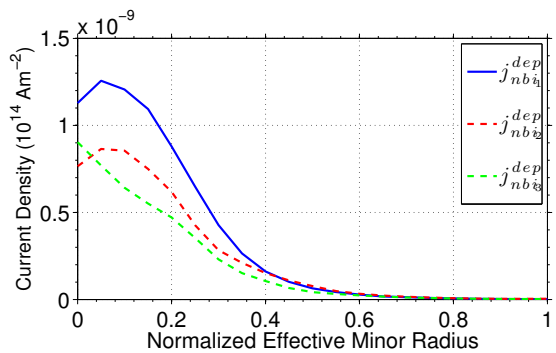

(f) $j_{nbi}^{dep}(\hat{\rho})$

Fig. 8: Reference (a) magnetic configuration parameters, (b) bootstrap current coefficients, (c) electron density and temperature profiles, (d) electron temperature and plasma resistivity constants, (e) NB deposition constants for the beamlines and (f) NB deposition profiles for the beamlines

Qualitative Agreement of Various Plasma Profiles in between the FPD Model and TRANSP Output

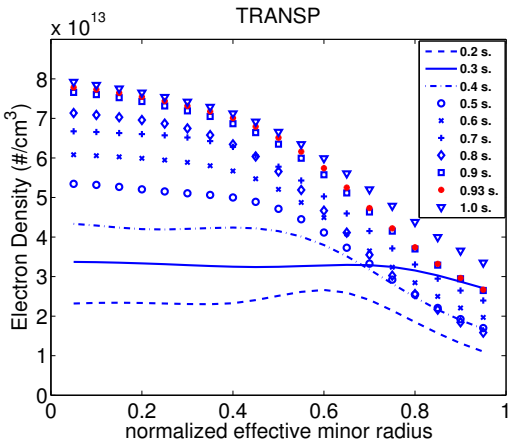

(a) $n_e(\hat{\rho})$ - TRANSP

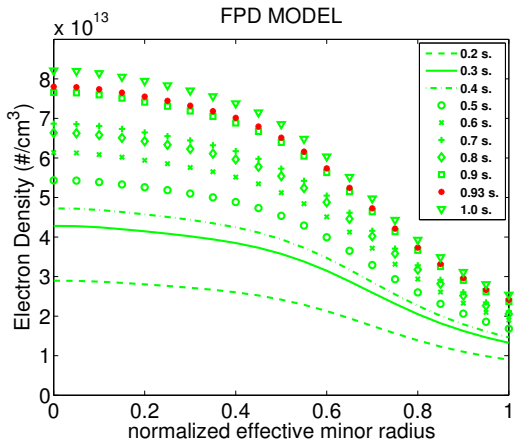

(b) $n_e(\hat{\rho})$ - FPD model

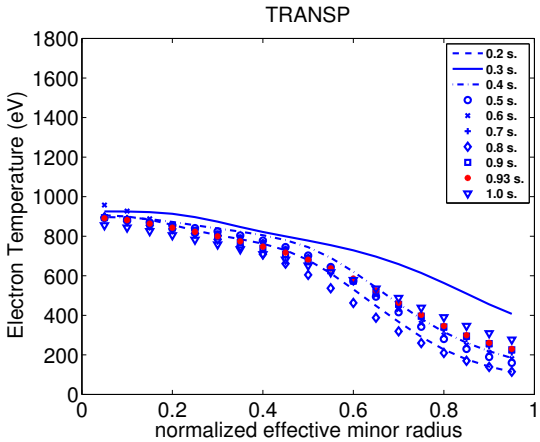

(c) $T_e(\hat{\rho})$ - TRANSP

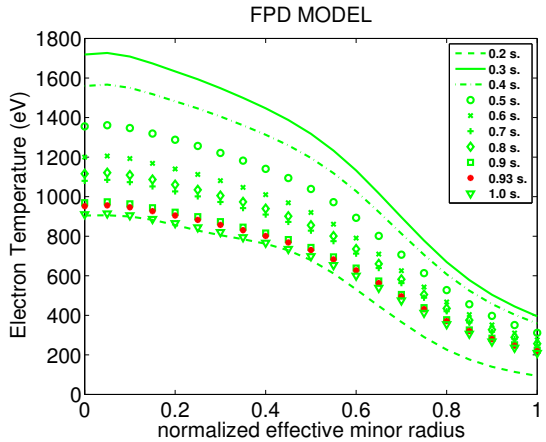

(d) $T_e(\hat{\rho})$ - FPD model

- NOTE: T_e profile exhibits some mismatch especially in the inner part of the plasma. This issue requires further analysis to address.

Neutral Beam Current Density Profile Comparison

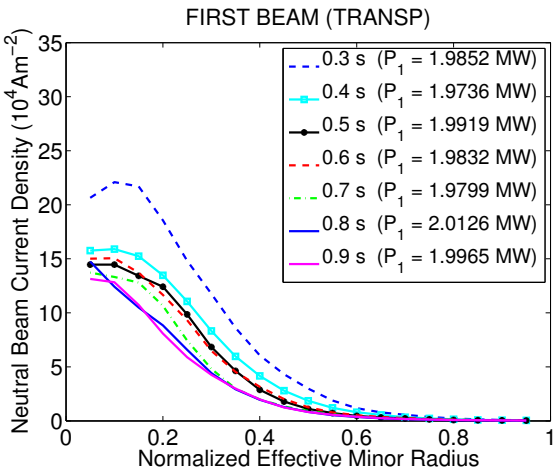

(e) 1^{st} Beamline (TRANSP)

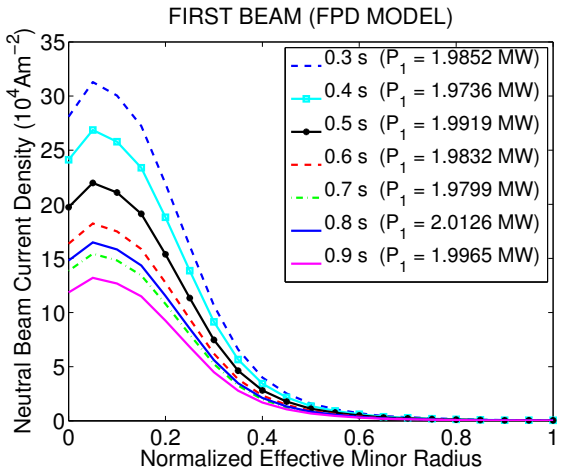

(f) 1^{st} Beamline (FPD Model)

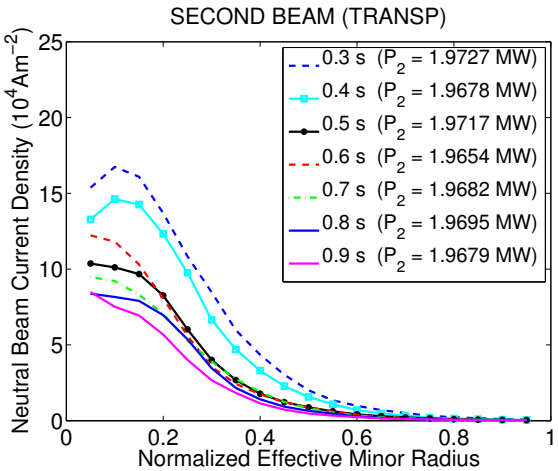

(g) 2^{nd} Beamline (TRANSP)

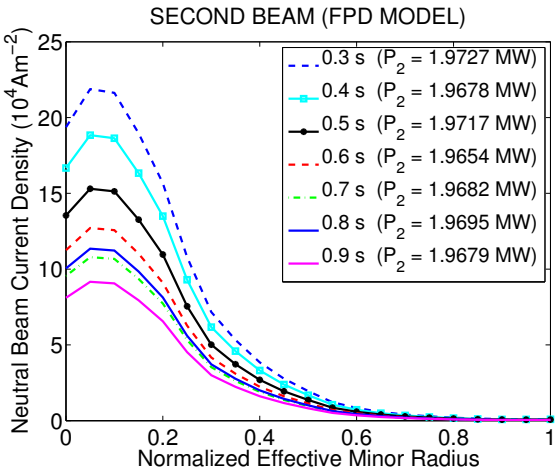

(h) 2^{nd} Beamline (FPD Model)

- NOTE: Increasing beam power does not always create an increase in the current density profiles.

NB and Bootstrap Current Density Profile Comparison

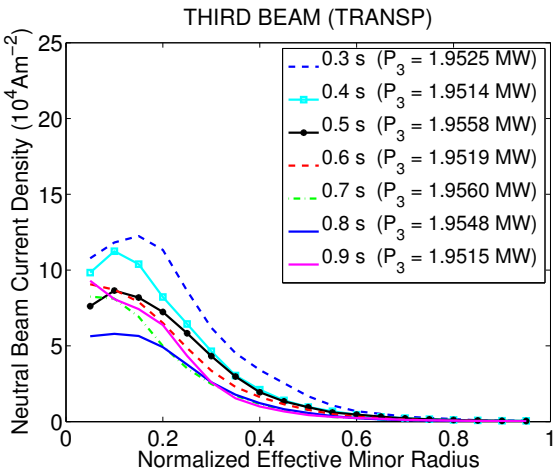

(i) 3^{rd} Beamline (TRANSP)

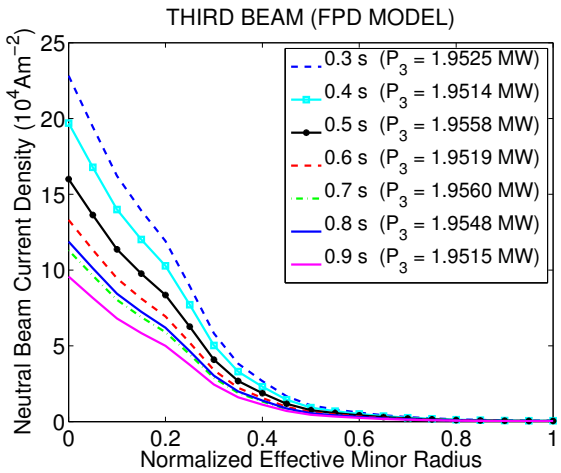

(j) 3^{rd} Beamline (FPD Model)

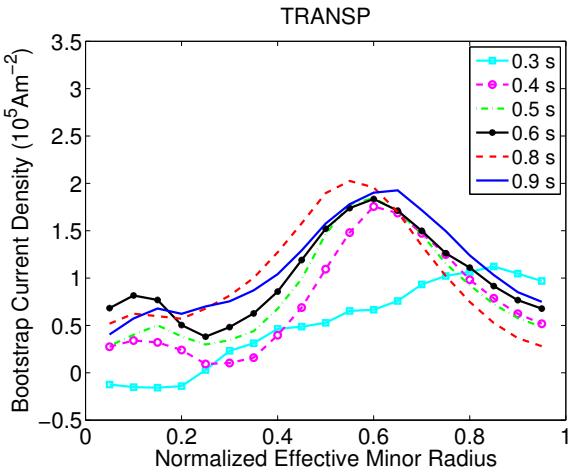

(k) Bootstrap (TRANSP)

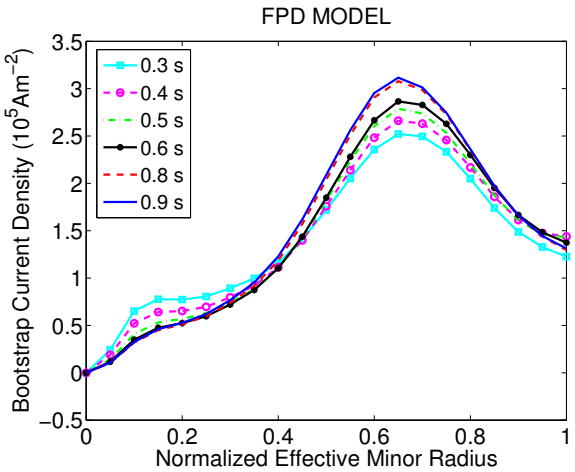

(l) Bootstrap (FPD Model)

Fig. 11: NB current density profile evolution comparison for the 3^{rd} beamline: TRANSP (i), and FPD model (j). Bootstrap current density profile comparisons: TRANSP (k) and FPD model (l).

Poloidal Flux Profile Comparison - $\psi(\hat{\rho})$, at fixed time

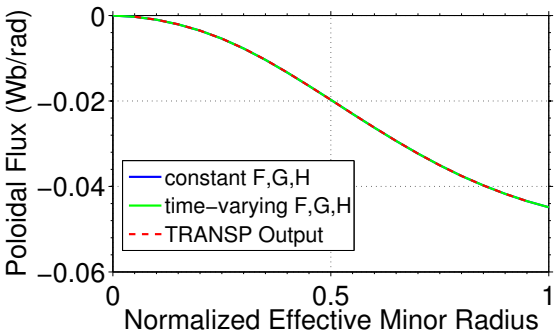

(a) $t = 0.2$ sec.

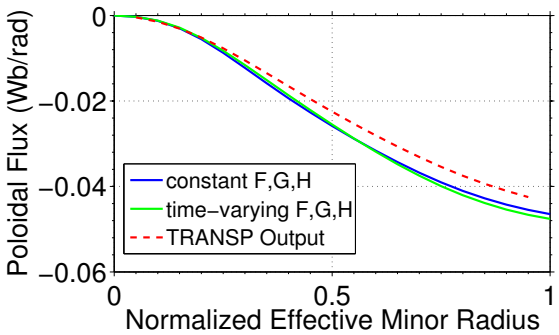

(b) $t = 0.4$ sec.

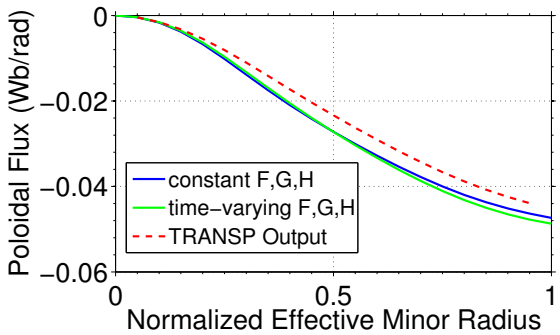

(c) $t = 0.5$ sec.

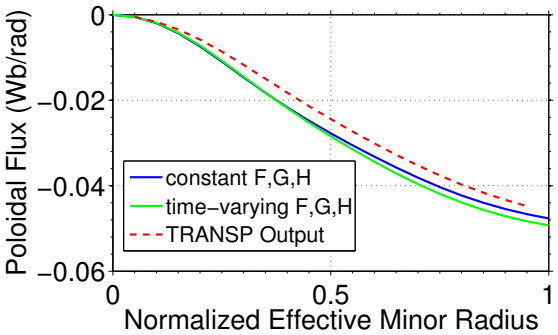

(d) $t = 0.6$ sec.

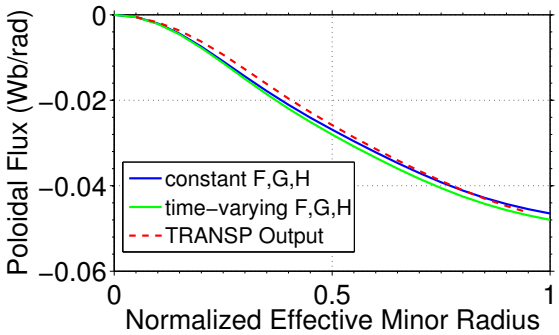

(e) $t = 0.8$ sec.

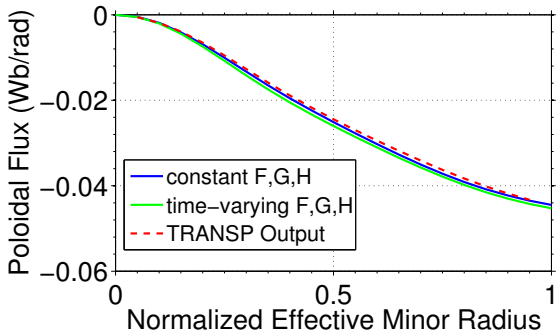

(f) $t = 1.0$ sec.

Fig. 12: Poloidal magnetic flux profile evolution comparison.

Poloidal Flux Comparison - $\psi(t)$, at fixed radius

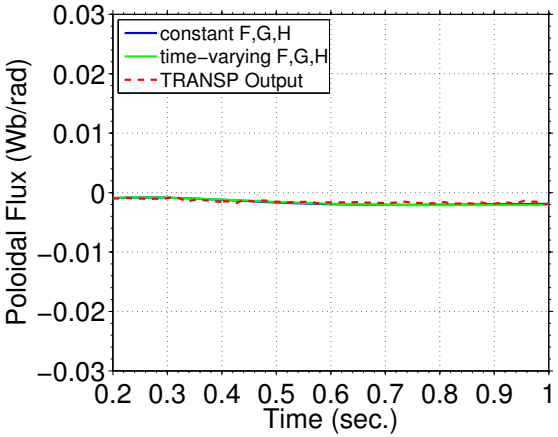

(a) $\hat{\rho} = 0.1$

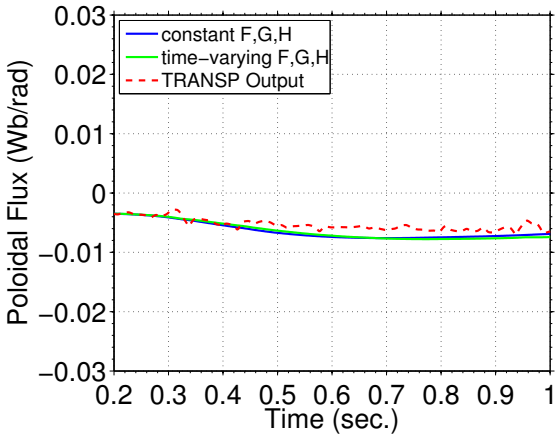

(b) $\hat{\rho} = 0.2$

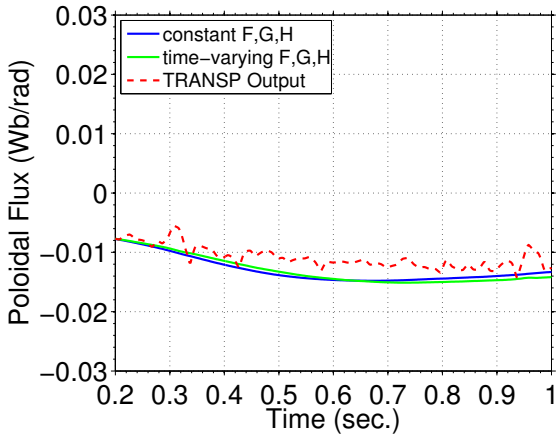

(c) $\hat{\rho} = 0.3$

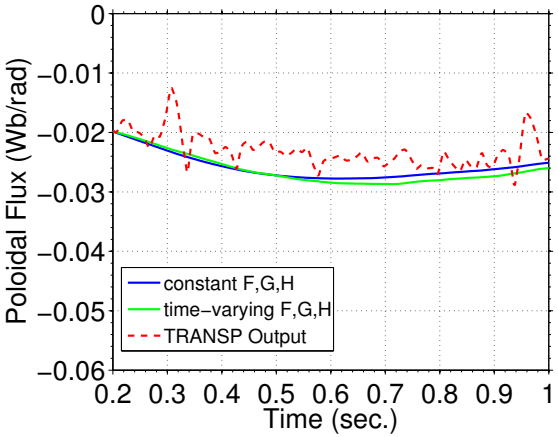

(d) $\hat{\rho} = 0.5$

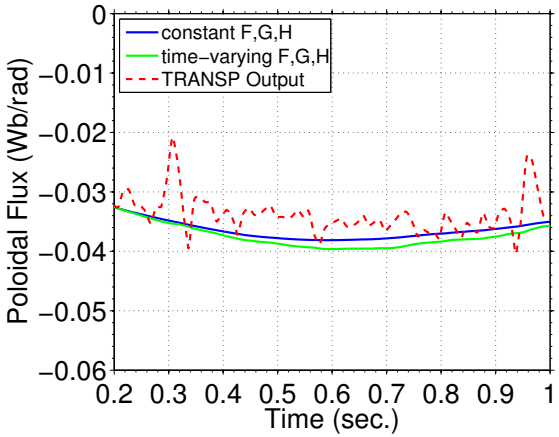

(e) $\hat{\rho} = 0.7$

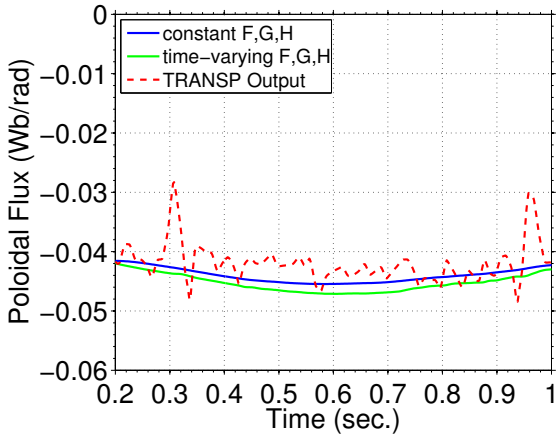

(f) $\hat{\rho} = 0.9$

Fig. 13: Poloidal magnetic flux evolution comparison.

Safety Factor Profile Comparison - $q(\hat{\rho})$, at fixed time

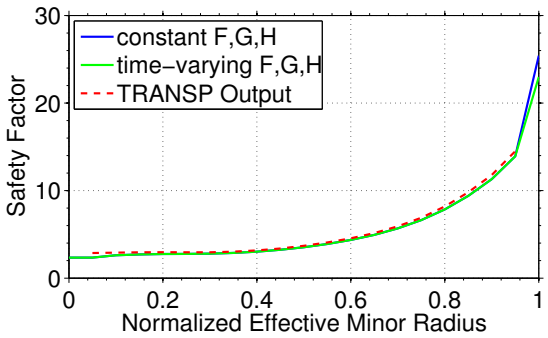

(a) $t = 0.2$ sec.

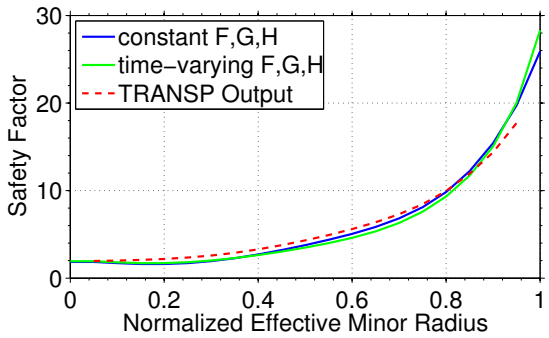

(b) $t = 0.4$ sec.

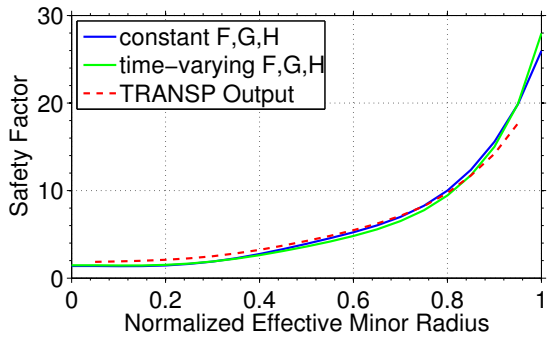

(c) $t = 0.5$ sec.

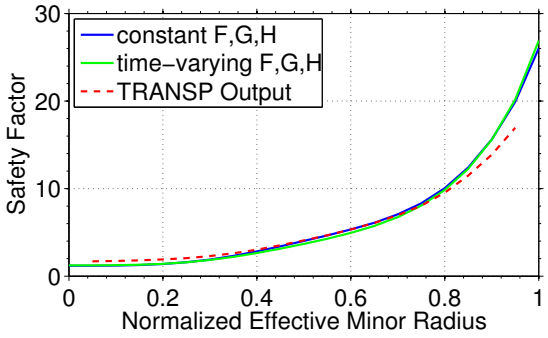

(d) $t = 0.6$ sec.

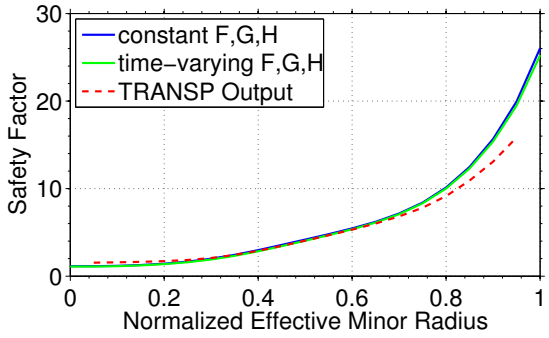

(e) $t = 0.8$ sec.

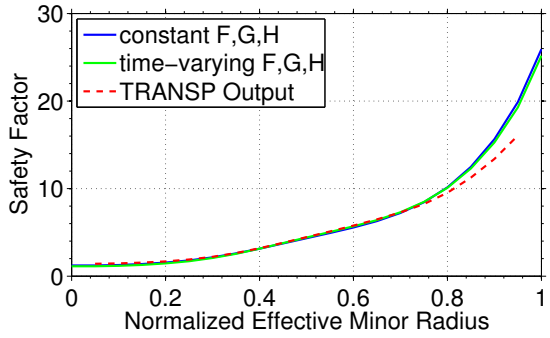

(f) $t = 1.0$ sec.

Fig. 14: Safety factor profile evolution comparison.

Safety Factor Comparison - $q(t)$ at fixed radius

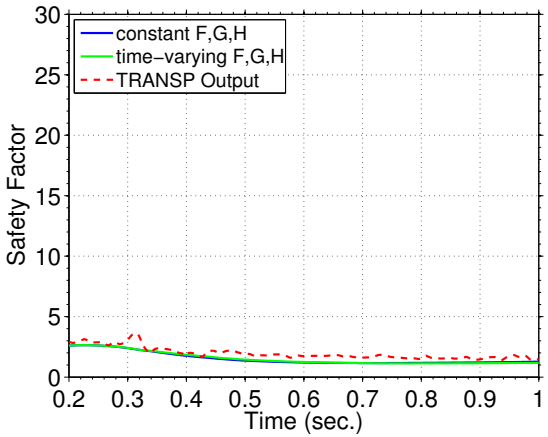

(a) $\hat{\rho} = 0.1$

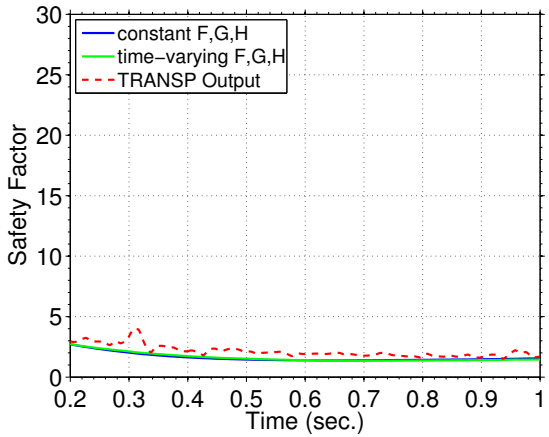

(b) $\hat{\rho} = 0.2$

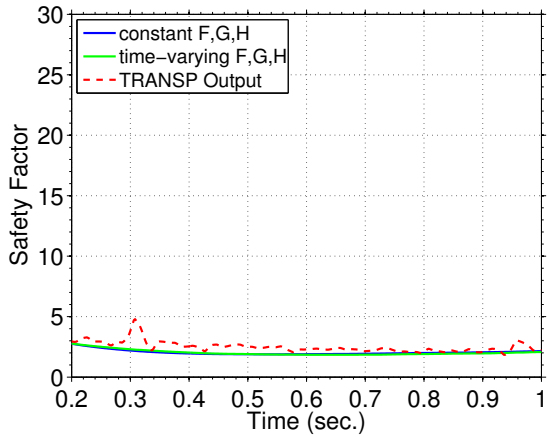

(c) $\hat{\rho} = 0.3$

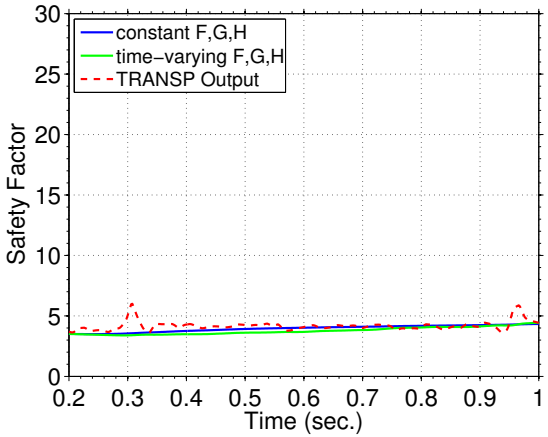

(d) $\hat{\rho} = 0.5$

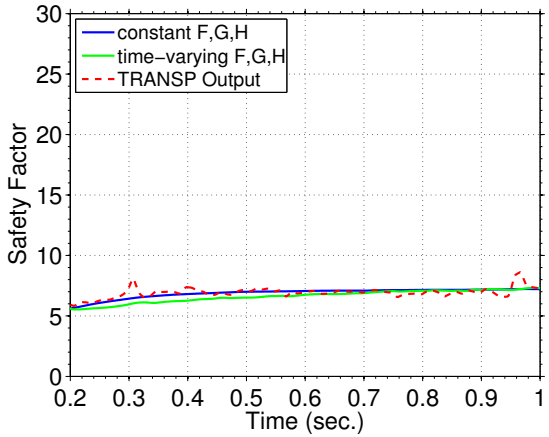

(e) $\hat{\rho} = 0.7$

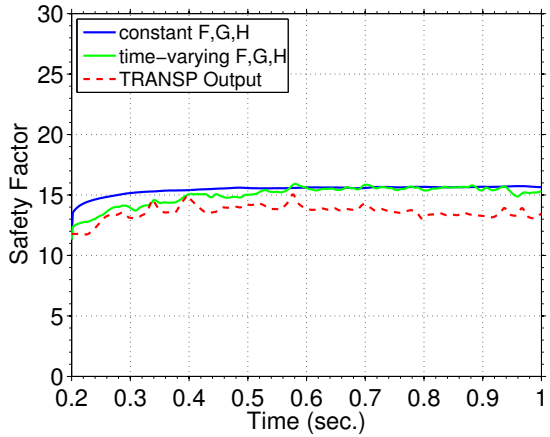

(f) $\hat{\rho} = 0.9$

Fig. 15: Safety factor evolution comparison.

Possible Uses of Control-oriented Model

1. Feedforward Control Design:

- Achieve target plasma state evolution throughout discharge by specifying actuator waveforms offline (actuator trajectory offline optimization), with goal of supporting experimental effort on scenario development.
- Study effects of different auxiliary heating/current-drive schemes on the ability to achieve a certain plasma state.

2. Feedback Control Design:

- Track target plasma state evolution and reject effects that external disturbances have on plasma dynamics, with goal of running repeatable discharges.

3. Plasma State Observers:

- Simulate model in real-time/faster-than-real-time as discharge evolves to obtain current/future plasma state for feedback control and disruption mitigation. Simulations can also be constrained by real-time partial (noisy) measurements of plasma state.

Schematics of Plasma Profile Control Applications

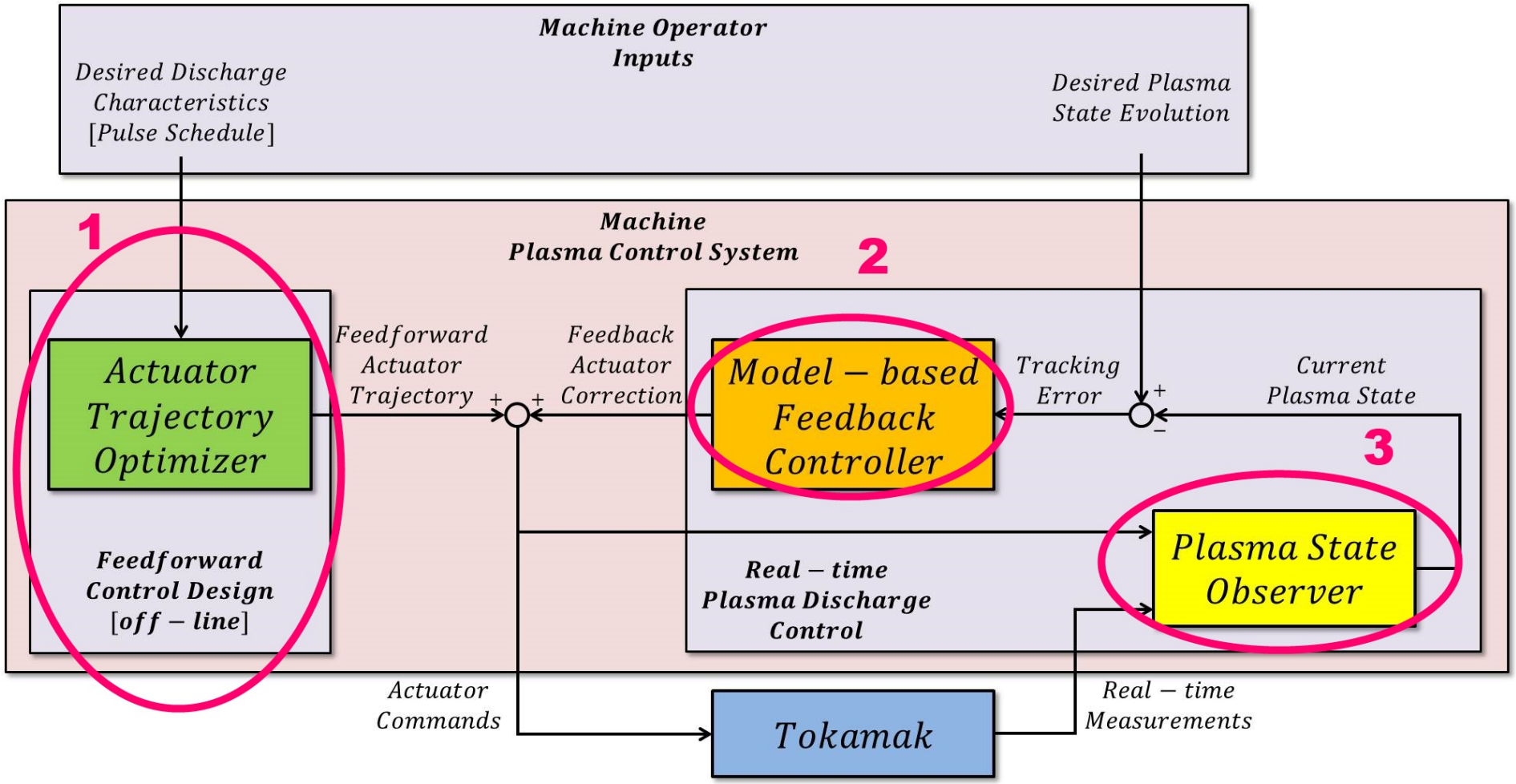

Fig. 16: Plasma profile and parameter control components.

Conclusions

- The nonlinear magnetic-diffusion PDE has been coupled with empirical models for the electron density, electron temperature, plasma resistivity and non-inductive current drive (neutral beams and bootstrap) to produce a first-principles-driven (FPD) control-oriented model of the current profile response in NSTX-U.
- The control-oriented model has been recently updated to enable:
  - Separate modeling of each beamline, adding more control design flexibility.
  - Time-varying modeling of magnetic geometry, increasing model accuracy and providing a mechanism for integration with plasma shape control.
- Predictions by the FPD control-oriented model show reasonable (for the purpose of control design) agreement with TRANSP simulations. Further analysis is still needed to explain some observed mismatches.
- A numerical integration scheme for the FPD control-oriented model has been coded in Matlab/Simuling to run simulations during the control design stage, and in C language to run Simserver simulations during the control implementation stage.